

On-Axis Polarization Calibration with the ATA

Casey J. Law, UC Berkeley

Mattieu de Villiers, SKA South Africa

28 October 2010

1. Abstract

We describe the properties and processing of on-axis polarimetric data from the Allen Telescope Array (ATA) between 1 and 3 GHz. The basic steps of the calibration process are presented, including detailed commands and scripts appropriate for MIRIAD users. We find that the relative xy phase of the array changes by roughly $1^\circ/\text{MHz}$, indicative of a physical delay between the x and y polarizations of the ATA feeds. The size of this delay and its change between epochs suggests it is partly related to the digital hardware. We also show that antenna polarization leakage is of order 10% and traces loop-like patterns in real-imaginary space as a function of frequency. The leakage changes by a few tenths of a percentage point per MHz, which requires polarimetric calibration in segments no larger than roughly 10 MHz. The period of leakage structures are similar to that of the log-periodic feed, which suggests that the leakage is caused by the design of the feed. The total polarimetric response of the array (both xy phase and leakage) changes discretely during changes to the hardware configuration, which occurs on month-long time scales. Within a single configuration of the digital hardware, the polarimetric calibration solutions may be copied between observations without inducing significant Stokes errors. Transferring solutions between different configurations of the digital hardware will introduce polarization errors of roughly 10% of the polarized intensity and systematically bias rotation measures.

2. Introduction

The ATA is demonstrating design concepts for radio interferometers that can be powerful in the study of polarized sources. Its wide bandwidth and flexible digital hardware give it access to a range of physics of polarized sources. The ATA is already being applied to Faraday rotation studies of radio galaxies over a range of frequencies (Law 2010).

While the promise is great, the novel design of the ATA requires a thorough vetting. Figure 1 shows the ATA signal path. Does the novel feed design have prohibitively large

polarization leakage? What calibration algorithm is needed to properly characterize the array? What kind of systematic errors could limit the science applications? This memo explores these questions with a series of observations of calibrators. All calibration in this memo is performed with sources at the phase and pointing center; a second memo explores the off-axis dependence (de Villiers & Law 2010).

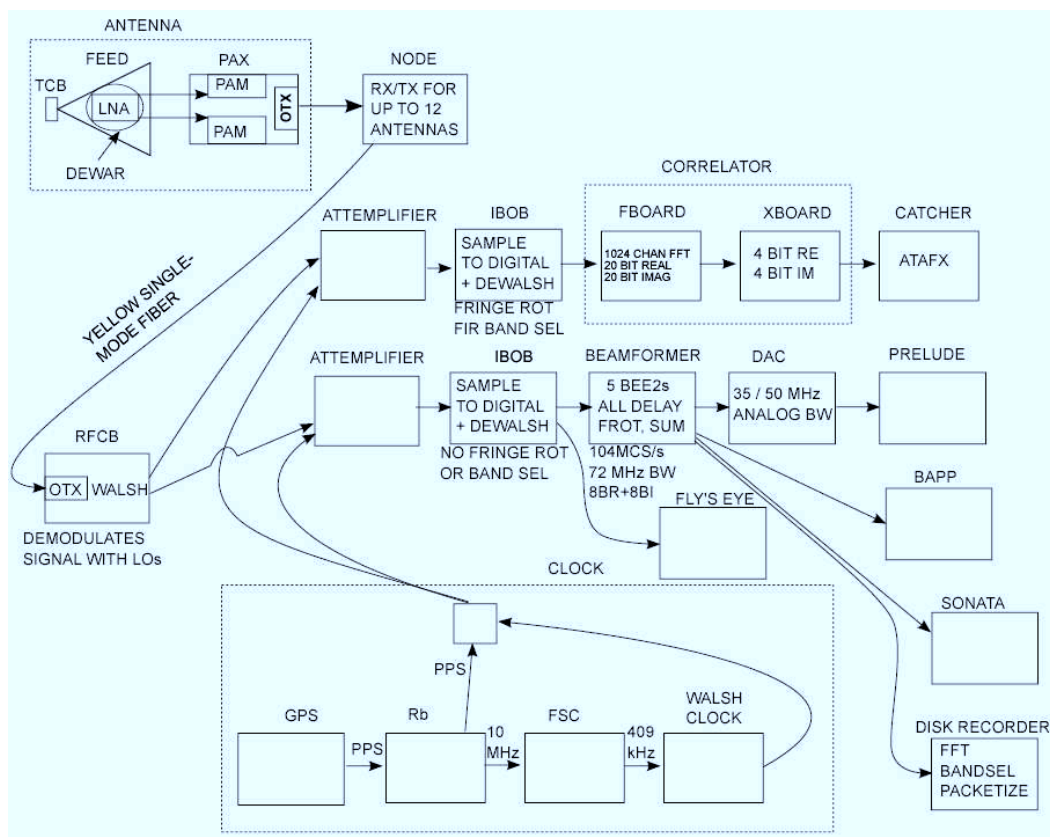


Fig. 1.— Diagram of the ATA signal path. Blocks show different physical components and arrows show the flow of data. All of the work presented in the memo comes from the correlator.

This memo shows how to polarimetrically calibrate the ATA for on-axis sources, the properties of the calibration solutions, and the quality of data after calibration. First, in §3, we describe the theory of polarimetric calibration. Section 4 shows the basic steps required to calibrate ATA data. In §5, we describe the systematic behavior of the calibration solutions, including a crude physical interpretation of the antenna leakages. Finally, §6 shows what quality polarimetric data one can expect from the ATA after applying this calibration technique.

3. Polarimetric Calibration Theory

Calibration is the process of measuring the Jones matrix describing the transformation of the true Stokes parameters into observed correlated data products. Typically this process is described by the linear equation $\vec{v} = \mathbf{J}\vec{e}$, where \vec{e} is the true Stokes parameter vector and \vec{v} is the observed data vector (Hamaker et al. 1996). In the case of linear feeds, the Jones matrix is formed by the matrix product as follows:

$$\mathbf{J} = \mathbf{G} * \mathbf{D} * \mathbf{C} * \mathbf{P} * \mathbf{S} \quad (1)$$

where \mathbf{G} represents the effect of antenna gain, \mathbf{D} is the “leakage” of the two feed polarizations into one another, \mathbf{C} is the rotation of the feed relative to the mount, \mathbf{P} is the rotation of the feed relative to the sky (the parallactic angle), and \mathbf{S} transforms the Stokes vector into the xy coordinate system.

The goal of the calibration process is to solve for the gain and leakage terms as a function of time and frequency. Expanding Equation 1 for a single baseline and folding the parallactic rotation term into the Stokes vector gives (Sault et al. 1996a):

$$\begin{pmatrix} v_{xx} \\ v_{xy} \\ v_{yx} \\ v_{yy} \end{pmatrix} \approx \frac{1}{2} \begin{pmatrix} g_{xx} & g_{xx} & 0 & 0 \\ g_{xy}(d_{1x} - d_{2y}^*) & 0 & g_{xy} & ig_{xy} \\ -g_{yx}(d_{1y} - d_{2x}^*) & 0 & g_{yx} & -ig_{yx} \\ g_{yy} & -g_{yy} & 0 & 0 \end{pmatrix} \begin{pmatrix} I_{rot} \\ Q_{rot} \\ U_{rot} \\ V_{rot} \end{pmatrix} \quad (2)$$

This shows that there is a degeneracy between some gain and leakage parameters. This degeneracy prevents us from measuring the system parameters with a single set of correlated data products with a known set of true Stokes parameters. As is well known today, the way around this degeneracy is to observe the calibrator over a range of parallactic angles, effectively providing multiple sets of observed and true values with a single set of systematic effects.

4. Basic Polarimetric Calibration

This memo discusses results from four observations in the middle of 2009. Observations were made on March 22, April 19, August 19, and September 7. During this period, eight feeds were added and six were removed as a part of a refurbishment program. Our analysis uses at most 11 antennas with two, high-quality polarizations feeds available for the March 22 observation; the same feeds were used for all observations. Table 1 summarizes the data used for this memo, including the Stokes I image quality in a typical 5 MHz segment.

We use MIRIAD (Sault et al. 1996b) to solve the gains and leakages for all antennas as a function of frequency and time. As described in §3 and Equation 2, the standard polarization calibration observation must cover a range of parallactic angles. For most results presented here, 3C 286 was observed at 1.43 GHz near transit. This gave the data parallactic angle ranges greater than 90° . 3C 286 is an excellent polarimetry calibrator ¹ because it is bright (> 10 Jy at 1.4 GHz), constant, isolated, polarized ($\sim 10\%$), and a rotation measure of roughly zero (Rudnick & Jones 1983). 3C 138 is nearly as good a polarization calibrator for similar reasons, so we use it in a few cases for this memo. ²

For initial processing, we flagged the data using RAPID (Keating et al. 2009) and reordered the data using UVAVER. Without reordering, ATA data is not guaranteed to be in the proper time and polarization order. Finally, we confirmed that the header parameter “evector” is set to 1.570796 radians (90°); according to the MIRIAD standard, this is appropriate when the y polarization is oriented vertically (Sault et al. 1996b).

The basic calibration first requires a bandpass calibration with MFCAL. This step solves for the frequency-dependent gain for each antenna as a function of time. Note that MFCAL has no knowledge of polarization (either of source or system parameters), but it makes some assumptions. The basic assumption is that the x and y polarizations should have similar phases after running MFCAL. For a weakly-polarized source, this allows one

¹See <http://www.vla.nrao.edu/astro/calib/manual/polcal.html>; R. Perley & N. Killeen, private communication

²Initially this memo made extensive use of 3C 138. We discovered that the leakage solutions based on 3C 138 and 3C 286 consistently different from each other, which indicated that the source model for one of these sources was wrong. Since 3C 138 is less commonly used as a polarimetric calibrator, we replaced most results derived from it with those of 3C 286.

Table 1. Summary of Observations

Day	Source	Duration (hours)	Good Antennas (alone, w/March 22)	Sensitivity (mJy; in 5 MHz)
March 22	3C 286	3.9	11, 11	22
April 19	3C 286	3.8	11, 11	22
August 19	3C 286	0.3	10, 7	58
September 7	3C 286	0.2	11, 6	65

to sum the two polarizations for higher signal to noise. Effectively, this assumption splits the array into an x and y array that are calibrated independently. For polarized sources, calibrating with this assumption will lead to gain errors of order the polarization fraction.

With the bandpass determined, the second calibration step uses GPCAL. This calibration tool can solve for the antenna-based gain and leakage as a function of time. However, GPCAL has no knowledge of frequency dependence, so it must be preceded by MFCAL. When solving for system parameters with data with a large polarization fraction ($> 5\%$), two optional arguments must be used. First, the “xyref” option tells GPCAL to solve for the xy phase offset for all antennas. Second, the “polref” option tells GPCAL to solve for the X leakage of all antennas, including the reference antenna. As shown below, the xy phase and leakage is nonzero for all antennas. The default assumption is often made because it is difficult to solve all leakages and phase offsets without a strongly-polarized calibrator observed over a wide range of parallactic angle.

These calibration steps can be applied using c-shell scripts in the MMM code repository³. Script “leak-cal.csh” will ensure data order, split data in frequency, and run MFCAL and GPCAL with appropriate options. As described in §5.2, the bandwidth must be split into at least 8 segments to resolve frequency-dependent leakage structure. This script also optionally outputs the leakage values into ASCII files that can be visualized with a Python plotting script called “plotleak-realimag.py”. The calibration solution for a calibrator can be applied to other observations with the script “leak-apply.csh”. In all cases, the scripts are relatively crude and should be edited before applying to data.

5. Properties of Calibration Solutions

Polarimetric calibration solves for the gain and leakage of each antenna polarization using a set of equations like Equation 2. Since gain and leakage are solved simultaneously, their solutions are interdependent. An error in one parameter will affect all others to some degree. Note that Miriad does not return a goodness of fit or errors for any of the solutions. The analysis presented here assumes that the data constrain the solution well.

³All scripts can be found with a web browser by prepending the name with “<http://svn.hcero.org/mmm/claw/>”. This analysis is based on svn revision number 925.

5.1. XY Phase

The phase alignment of the x and y portions of the feed is an important parameter for absolute polarization angle calibration. This parameter is often referred to as the “xy phase” and can only be solved in observations of a strongly polarized calibrator with known polarization angle. In all four observing periods, the xy phase drifts linearly with frequency. The rate of xy phase drift in the four observations at 1.43 GHz is (in chronological order): $0.84^\circ/\text{MHz}$, $0.86^\circ/\text{MHz}$, $0.92^\circ/\text{MHz}$, and $1.13^\circ/\text{MHz}$.

The non-zero phase drift implies that there is delay difference between the x and y polarizations of the feed. This delay may be related to the way the feed senses the electromagnetic wave, since the x and y tines of the feed are interleaved. If the xy phase is thought of as a delay, a drift of $1^\circ/\text{MHz}$ is equal to roughly 3 ns. The four measurements are similar, but show significant variation on month time scales. The delay is of the order of timing error introduced by the IBOB hardware that does the digital sampling. If the xy phase changes are tied to the IBOB hardware, it will change discretely during power cycling and updates to the digital programming, which occurs irregularly on month time scales.

5.2. Frequency Dependence of Leakages

Figure 2 shows the leakage derived for several antennas at 1.43 GHz from an observation of 3C 286. There is a distinctive loop-like structure to the leakage changes with frequency. Near 1.4 GHz, the leakages change with frequency at a rate of a few tenths of a percentage point per MHz. Across the typical 100-MHz bandwidth currently used by the ATA, the feed polarization response will change by tens of percentage points. The mean leakage amplitude for an individual antenna is about 9% with a scatter of about 2% introduced by the variation across the band at 1.4 GHz. Including all 11 antennas gives a similar mean, but a larger scatter of about 4%. The similar mean when averaging over many antennas shows that different antennas have some correlation in leakage values.

We repeated the observation of 3C 286 with two correlators observing at 1.43 and 1.48 GHz. These observations each have a bandwidth of 100 MHz and overlap by roughly 40 MHz. Figure 3 shows that the leakage is repeatable between correlators at the same frequency to within a few percentage points. This shows that the leakage does not originate in the LO system. We conclude that most of the leakage has its origin in either the antenna/feed or through crosstalk, the correlation of x and y signals in the ATA analog signal path.

The leakage loop period is similar to the period of the log-periodic feed (about 3/4 of a

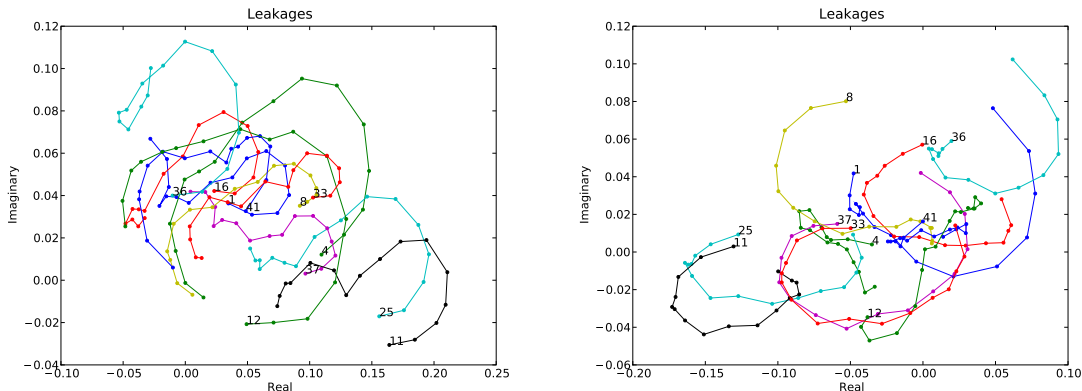


Fig. 2.— *Left*: Antenna-based, x-polarization complex leakages derived from an observation of 3C 286 at 1.43 GHz. Each colored line shows the leakage for a different antenna as a function of frequency. Each point on a line uses roughly 5 MHz of data. *Right*: The same as the left panel, but showing leakage for the y-polarization. The x and y polarization leakages have similar looping structures, but rotate in different directions.

turn near 1.4 GHz). One possibility is that most of the leakage is caused by the x and y feeds being non-parallel, either due to the pyramidal design or a bend in one of the feed lines. Figure 2 shows that the x and y polarization leakages seem to rotate with opposite handedness in the real-imaginary plane. This is consistent with the idea that — at least at 1.4 GHz — the leakage is dominated by the feed geometry.

If the leakage pattern is tied to the periodic nature of the feed, then we expect that the number of cycles completed per MHz would decrease with frequency. The log-periodic design has half as many cycles per 100 MHz for each doubling of frequency. Figure 4 shows the leakages from a new observation at 3.14 GHz. The 3.14 GHz leakages show less loop-like structure than at 1.43 GHz (Fig. 2), which supports the idea that the leakage pattern is tied to the physical design of the feed.

5.3. Leakage and Squint

As shown above, some portion of the leakage frequency-dependence is correlated between antennas (see also Law 2010). This behavior suggests that the ATA leakages can be affected by a system-wide effect. One possibility is that beam “squint”, or x and y beam pointing differences, can produce this effect. de Villiers & Law (2010) shows that leakage-induced errors become significant in snapshot observations for pointing errors of

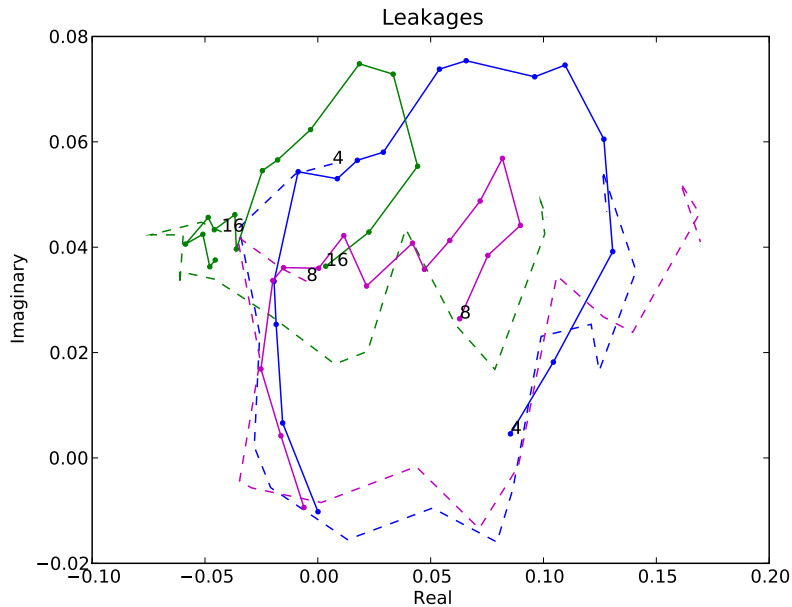


Fig. 3.— Leakages for three antennas in a dual-correlator observation at 1.43 and 1.48 GHz. The two bands overlap by roughly 40 MHz and show similar leakages at similar frequencies.

order half the half-power distance ($18'$ at 3.14 GHz). This is a factor of three larger than the typical antenna squint (MacMahon & Wright 2009), so it is possible that this effect contributes at frequencies higher than a few GHz. An alternative possibility is that the antennas have correlated leakages because it is a property of the feed design.

To distinguish between the pointing error and feed design origins of the leakages, we compare the measured feed squint to the mean leakage amplitude for several antennas in Figure 5. In general, there is no trend connecting the antenna squints and leakages. This plot does not exclude the possibility of a connection, since we know that leakages show large amplitude changes with frequency that may wash out structure in this plot. However, there is no strong correlation between feed squint and leakage amplitude, which suggests that the leakage structure is tied to the feed design.

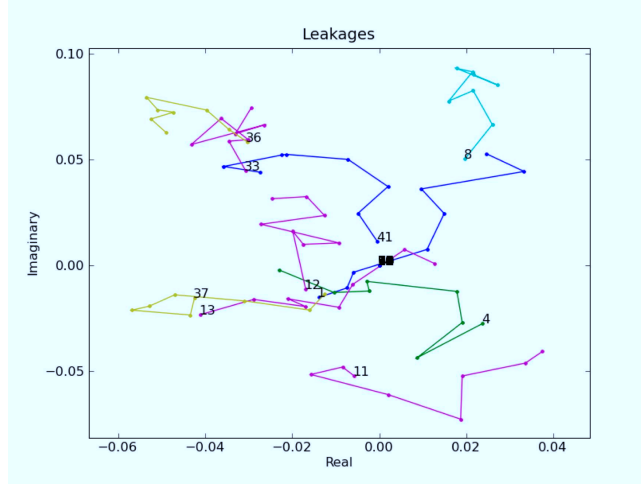


Fig. 4.— Complex leakages from an observation of 3C 138 at 3.14 GHz. Comparing to Figure 2 shows that the antenna leakages have less loop-like behavior at this higher frequency.

5.4. Time Dependence of Leakages

Figure 6 compares the leakage solutions at 1.43 GHz measured at all four epochs. All epochs had data spanning a wide range of parallactic angles, so they should have similar quality solutions (outside of RFI effects). In general, all four epochs have similar leakages within 0.05. In some cases, a few channels have leakage values deviant from the trend seen in other epochs. It is possible that the differing data quality between epochs may lead to different leakage solutions. To test this possibility, §6 shows the quality of transferred polarimetry calibration.

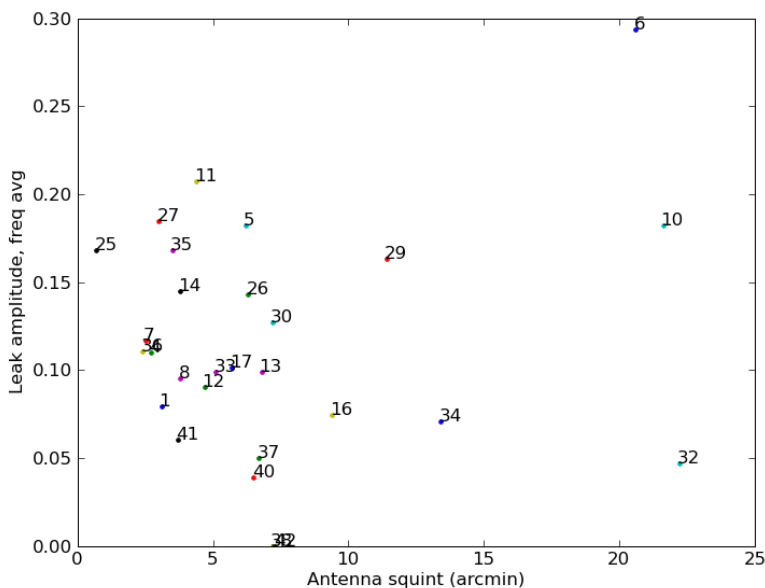


Fig. 5.— Comparison of antenna measured squint (pointing difference between x and y feeds) and antenna leakage in late 2009. The amplitude of the leakage was measured from calibrations across a 40 MHz band at 1430 MHz.

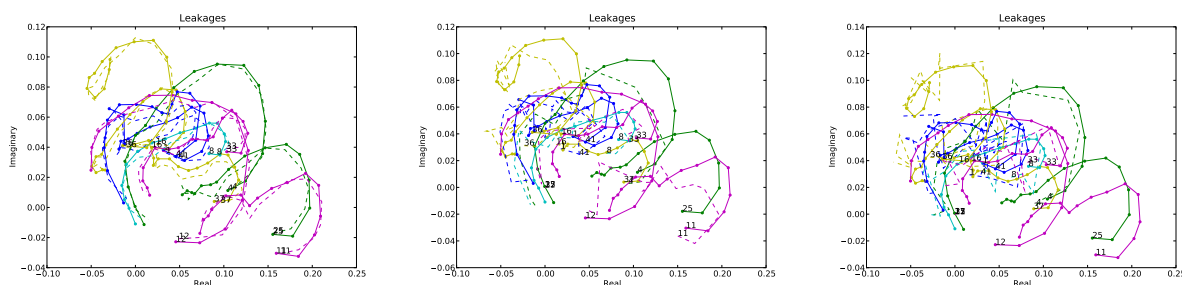


Fig. 6.— *Left:* Leakages for the x polarization in the real-imaginary plane for each antenna in two, 1.43 GHz observations. The solid lines show the leakage solutions for an observation of 3C 286 on March 22, while the dashed line shows the leakages from an observation on April 19. In cases where antennas were not present in both data sets, only one line is plotted. *Middle:* The same as the left plot, but the dashed line shows the leakages from an observation of 3C 286 in August 19. *Right:* The same as the left plot, but the dashed line shows the leakages from an observation of 3C 286 on September 7.

The March, April, and September epochs have leakages that are more similar to each other than to those measured in August. This may indicate that the August epoch was affected by RFI or a change to the digital hardware (a hypothesis tested in §6.3). At the least, it shows that there is no gradual change to the leakage pattern. The largest change in the leakage solutions between any of the four epochs is less than 4 percentage points, but the typical change is less than 2 percentage points.

6. Data Quality

6.1. Visualizing Visibilities

After applying calibration, it is good to check the calibration quality using UVPLT. The top of Figure 7 shows a plot of Stokes Q, U, and V versus parallactic angle for a set of baselines. Since these plots effectively derotate the apparent Stokes vector, the linear polarization should be constant despite the change in parallactic angle. These plots show that there is no systematic variation in the linear polarization as the antennas rotate relative to the source. Poorly calibrated data will show systematic behavior (a sine function) caused by false Stokes Q and U signals rotating in an unexpected way.

The bottom of Figure 7 shows another visualization of calibrated data quality. Plotting the average of all visibilities as real/imaginary points shows both that the flux density is correct and that errors are well behaved (Gaussian). Similar plots and a more extended discussion of ATA polarimetric data quality are given in Law (2010).

6.2. Stokes Errors from Leakage Errors

Calibrating assuming no frequency structure provides a test of the effects of frequency-dependent leakage and xy phase. We compare the mean linear polarization after calibrating assuming one and 16 frequency segments. Calibrating the March 22 data assuming a single band produces a systematic error of 25 ± 6 mJy, or 4% of the linear polarization.

This error likely understates the effect of leakage errors on RM studies. As shown in §5.2, the leakages form nearly complete loops in real-imaginary space at 1.4 GHz. Stokes errors induced over an entire loop will be smaller than over a segment of the loop. However, if one calibrated assuming no frequency structure, but studied the Stokes parameters on frequency scales less than the loop period, these errors would not average down. The RM

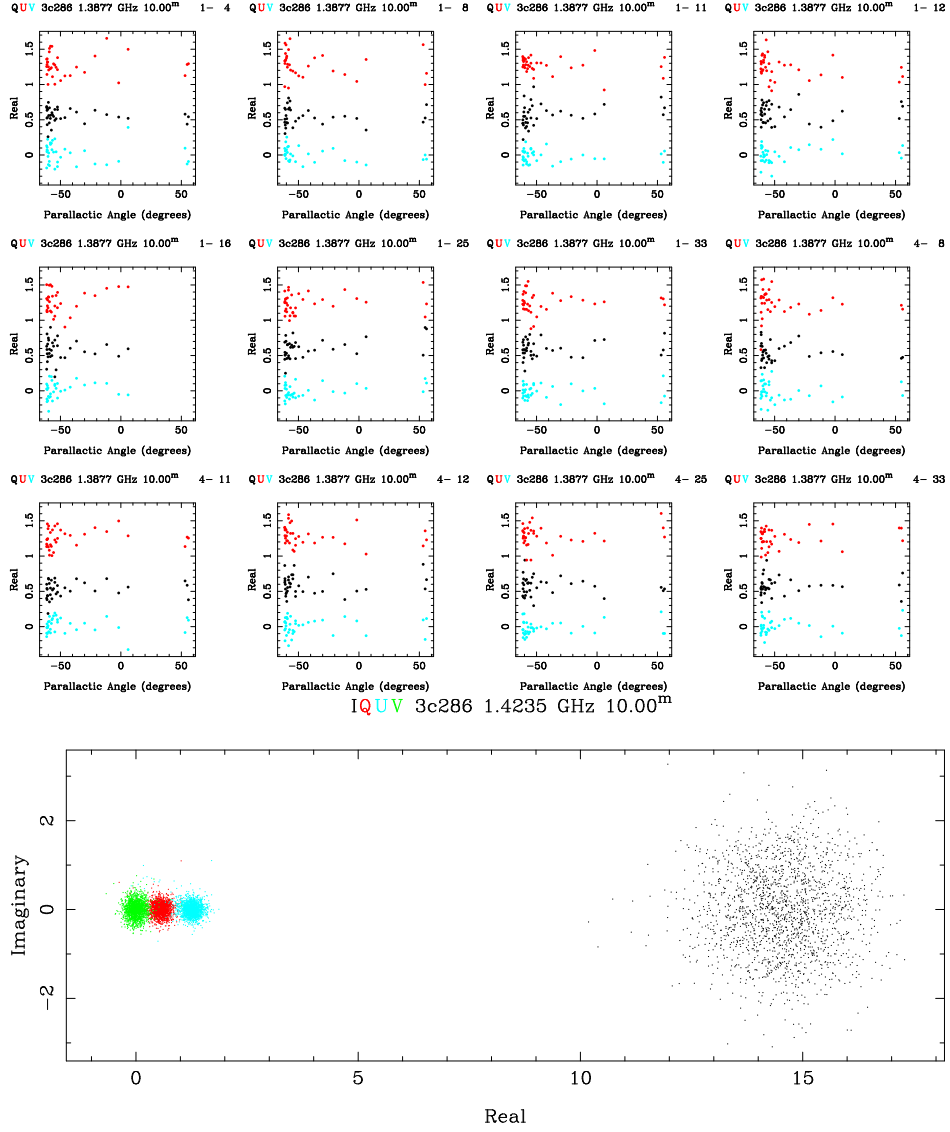


Fig. 7.— *Top*: Plot of Stokes Q (black), U (red), and V (blue) versus parallactic angle for a calibrated observation of 3C 286 near 1.4 GHz. Each window shows data from a single baseline; several representative baselines are shown. This plot shows little parallactic-angle dependence, which demonstrates that it is at least roughly calibrated. *Bottom*: Plot of the real and imaginary parts of the visibility for Stokes I (black), Q (red), U (blue), and V (green) in calibrated data of 3C 286. All Stokes parameters are symmetric points in real/imaginary space and located at the expected values, which shows that it is calibrated approximately correctly. The Stokes I points are much wider than the Stokes Q, U, and V probably because there is a few Jansky of flux in other sources in the primary beam.

measured at any part of the band would have a large contribution from leakage errors. Assuming linear scaling in the loop period, the effects of leakage errors are minimized for segments with bandwidth, $\Delta\nu \lesssim 10 \text{ MHz} * (\nu/1.4 \text{ GHz})$.

6.3. Transferring Polarization Calibration

The polarization response of the array may be related to the feed design or the digital hardware. If it is related to the feed design, most of the response should be stable in time (e.g., Fig. 6). We test this idea by transferring calibration from one time to another and measuring the errors in observed Stokes parameters and rotation measure (RM).

Transferring calibration can also show whether the time changes in the polarimetry solutions represent changes in the array response or errors in individual solutions.

We polarimetrically calibrated the four, 1.43-GHz observations using the technique described above. Each band was broken into 16, 5-MHz segments and calibrated for antenna-based gain, leakage, and xy phases. The blue points in Figure 8 show the result of fully calibrating each epoch individually.

To test for effects of polarimetric changes, the calibration was repeated with the leakage and xy phases fixed at the values found for the March 22 data. The antenna-based gain and bandpass were still solved for each epoch, but parameters related to the polarimetric response were kept fixed. This reproduces the effect of how one may polarimetrically calibrate by assuming stable xy phases and leakages, but use the frequent gain calibration typically available. Note that since the gain and leakage calibration are solved simultaneously, any error in gain error in the March 22 data will create errors in the leakage applied to other datasets. This error may not be visible to traditional error analysis, but will appear in this test.

Figure 8 summarizes the effect of this calibration approach. The arrows show the complex Stokes error vectors (Stokes Q and U) observed as a fraction of the total polarized flux. Table 2 quantifies this comparison in another way, including a measurement of the apparent RM⁴. The table and figure show that transferring the March 22 polarization calibration to April 19 produces systematic errors smaller than 1% of the polarized flux. However, transferring polarization calibration from March to the August and September observations produces very significant errors.

The observed Stokes changes are similar to the change in xy phase between these epochs

⁴We measure the RM using the “RM synthesis” technique (Law 2010)

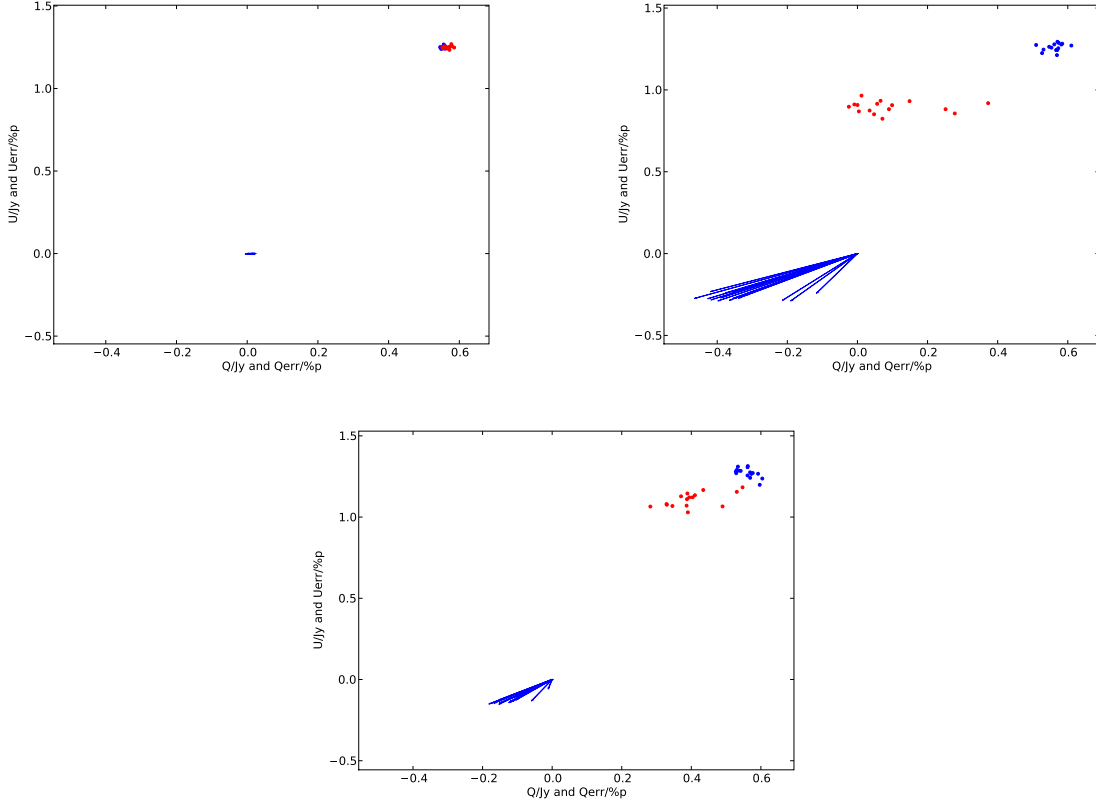


Fig. 8.— Three plots showing the polarization accuracy under two calibration solutions. *Top:* The points show Stokes Q and U of 3C 286 for each 5 MHz segment from April 19. The blue points show the results when calibration is derived from the April 19 data, while red points show results after applying polarization calibration (leakage and xy phase) from March 22. The arrows show the difference between the red and blue points normalized by the true polarized flux. The arrows essentially show a normalized Stokes error vector. *Middle:* Same as the left panel, but for calibration applied to the August 19 data. *Bottom:* Same as the left panel, but for calibration applied to the September 7 data.

(§5). However, while the leakages are similar between the March, April, and September data, the September epoch has a significant systematic Stokes error. This suggests that the xy phase drift contributes most of the September Stokes error, while the leakage changes contribute further to the August Stokes error. The large Stokes error for the August epoch shows that the leakage solutions are genuinely different then, and not an artifact of RFI.

These results show that the changes in the solutions are due to changes in the response of

the array that becomes significant over time scales longer than a month. The combination of xy phase and leakage solutions with the Stokes errors shows that at least part of the calibration depends on the digital system. The alignment of the x and y signals in the digital domain is reset when the digital hardware is reset, which is roughly monthly. However, some portion of the polarization calibration is tied to the feed design, which is stable over time scales of several months.

7. Conclusions

We have described the calibration process and presented the properties of on-axis polarimetric data from the ATA. For frequencies from 1 to 3 GHz, the ATA has polarization leakage of order 10%. While this is larger than typical with other radio telescopes, we find that standard polarimetric calibration techniques can remove this systematic effect. The polarimetric response has significant frequency structure on scales larger than 10 MHz. This requires breaking the nominal 100 MHz bandwidth into segments and applying calibration on each segment. The polarimetric response of the array (xy phase alignment and leakages) are likely caused by both the digital hardware and the physical design of the feed.

The polarization calibration solutions change irregularly, but typically on time scales longer than one month. For a single hardware state, the transferring calibration solutions produces systematic errors at the level of a one percent of the polarized flux at 1.43 GHz. When transferring calibration solutions for different hardware states, the systematic errors rise to more than 10 percent of the polarized flux. These errors produce false rotation measure signatures of order 10 rad m^{-2} . Tracking the configuration of the hardware will be critical to transferring calibration solutions.

Future work may be able to develop a physical model for the origin of the leakage frequency structure. As yet, we cannot exclude the possibility of crosstalk of the analog signals affecting the leakages. Comparing leakages after feed swaps or between antennas with different analog signal paths can test this.

We thank the MMM group at UC Berkeley and Billy Barott help with various aspects of this project.

Table 2. Polarimetric Calibration Quality for Custom and Transferred Solutions

Day	Custom Cal.	March 22 Pol. Cal.	
	RM (rad m ⁻²)	RM (rad m ⁻²)	Frac. Stokes Error % p
March 22	0.0±0.3	—	—
April 19	-0.1±0.3	-0.1±0.5	1
August 19	1.2±1.5	-12.4±5.4	43
September 7	-1.1±1.9	-8.2±3.4	17

REFERENCES

- de Villiers, M. & Law, C. 2010, Wide field polarization calibration in the image plane using the Allen Telescope Array, Tech. rep., University of California, Berkeley
- Hamaker, J. P., Bregman, J. D., & Sault, R. J. 1996, *A&AS*, 117, 137
- Keating, G., Barott, J., & Allen Telescope Array Team. 2009, in *American Astronomical Society Meeting Abstracts*, Vol. 214, American Astronomical Society Meeting Abstracts
- Law, C. J. 2010, ArXiv e-prints
- MacMahon, D. & Wright, M. 2009, *Antenna Gain, Pointing, Primary Beam and Bandpass Calibration*, Tech. rep., University of California, Berkeley
- Rudnick, L. & Jones, T. W. 1983, *Astron. J.*, 88, 518
- Sault, R. J., Hamaker, J. P., & Bregman, J. D. 1996a, *A&AS*, 117, 149
- Sault, R. J., Killeen, N. E. B., & Kesteven, M. J. 1996b, *AT Polarization Calibration*, Tech. rep., ATNF